OTC 23343-PP

Ocean Observing in the 4th Dimension--Using Autonomous Gliders for Operational Surveillance of the Gulf of Mexico

Peter Brickley, Jim Feeney, Benjamin Shaw, Glenn Burnett, Patrice Coholan, Horizon Marine, Inc.

Abstract

The ocean circulation in the Gulf of Mexico is highly dynamic in four dimensions (4D). The circulation varies throughout the interconnected shelf, slope, and deep ocean domains (3 dimensions) and varies greatly in time (the 4th dimension). Obtaining timely, comprehensive, and accurate forecasting of this 4D system remains a challenge for operators on the outer continental shelf (OCS). Long-range autonomous underwater gliding vehicles (AUGVs) enable collection of high spatial resolution sections through the ocean repeatedly, autonomously, and at a very low cost compared to conventional methods. Using these new tools, in-situ data can be continuously assessed to provide a more integrated description of the ocean state. We describe a series of glider observations obtained during extended (3.4 months) observational campaigns in the eastern Gulf of Mexico. One survey period took place from April-August 2011, covered a linear distance of 1400 nm (2700 km), and collected over 1000 vertical profiles to 1000 m. The deployment spanned the Loop Current (LC) growth phase and detachment of Eddy Hadal. Several cross-sections were obtained through the LC front, cyclonic frontal eddies, and in close proximity to working platforms in lease areas of the NGOM slope. The in-situ fields of ocean density help to delineate the subsurface boundaries of these dynamic features, and their geostrophic velocity structure can be inferred from lateral density variations. Sustained in-situ glider observations throughout the eastern Gulf of Mexico will improve the knowledge and forecasting vital for efficient day-to-day operational management decisions of the offshore petroleum industry.

Introduction

At basin scales, the ocean circulation in the GOM is dominated by the Loop Current. The Loop Current extends northward from the Yucatan Channel into the GOM and connects to the Florida Straits. At times, it extends well north over the upper continental slope before retroflecting to the southeast and exiting the Gulf. Periodically the LC retroflection will pinch and form a closed recirculation of water that may ultimately detach (or shed) as a Loop Current Eddy (LCE) at intervals from 3-18 months (Forristall, et al., 1992, Leben et al., 2005, Sturges et al., 2005). The LC and LCE are deep structures extending down to nearly 1000 m, and both exhibit strong surface currents in excess of 3.75 knots (2 m/s). The LC and its energetic eddies will, at times, exert a strong influence on the NGOM upper slope and shelf due to the interconnected nature of circulation. A variety of physical mechanisms can potentially influence LC intrusion and eddy separation, including instability of the LC within the GOM and upstream effects propagating though the Yucatan Channel. Loop Current Frontal Eddies (LCFEs) typically form along the western part of the LC and amplify in an unstable manner as they propagate downstream along the LC (Vukovich and Maul, 1985), exerting a strong influence on the LC position and evolution. Strong ocean currents encountered in any part of the Outer Continental Shelf (OCS) and deeper waters can significantly threaten the safe and efficient completion of deepwater drilling operations, creating unexpected downtime and added risk. Deepwater operators on the OCS require more accurate prediction on the LC and LCE location, intensity, and migration at meso- and even smaller scales (100 m – 10 km).

Monitoring and forecasting the LC frontal development and evolution depends on the accurate, timely collection of real-time observational data. The surface expression of the LC intrusion and eddy detachment and separation events are observable at synoptic scales in several remotely sensed fields such as sea surface temperature (SST) and sea surface height (SSH). These methods are frequently limited by atmospheric conditions, limited coverage, and sensor resolution, respectively. This

problem becomes acute for obtaining reliable data on the mesoscale LCFEs. Extensive use of satellite-tracked Lagrangian drifters in conjunction with remote sensing data has proven a more reliable means to delimit the major circulation features. The variable duration of drifter residency within features of interest creates gaps in coverage, sometimes at critical periods, and necessitates regular drifter replacement. Despite many advances in recent years, these methods provide incomplete knowledge of the LC/LCE location, movement, and evolution of the frontal regions because information about the subsurface structure of these features is limited. Improved prediction of the LC behavior is gained though in-situ oceanographic measurements acquired at sufficient spatial resolution to form a comprehensive view of the LC system throughout the water column. Collecting data from the ocean interior is an expensive and exhaustive process. Large research vessels, expensive mooring arrays, a crew of technicians, and a great deal of time are needed to obtain the high resolution in-situ data needed to fully describe the 4D ocean interior. Long-range autonomous underwater gliding vehicles (AUGVs) offer a means to collect high resolution in-situ ocean data repeatedly, autonomously, and at a very low cost compared to conventional methods.

Autonomous Ocean Gliders

AUGVs are purposely designed to be small and slow to avoid the high penalty in frictional drag imposed on faster moving objects (**Figure 1)**. Gliders are designed to move slowly through the ocean for months at a time, continuously returning data gathered over thousands of kilometers. They are a more cost-effective solution for data collection than vessel-based systems and can investigate larger scale phenomena than is possible with moored instruments.

AUGVs are driven by a simple buoyancy engine. The vehicle volume is manipulated by an internal pump to become either heavier or lighter than the surrounding water. In the descending (or ascending) glide phase, the sinking (or rising) motion is converted to forward thrust by the two wings. The glide trajectory is along angles of 18° to 25° from horizontal and at forward speeds of 25 to 35 cm/s, producing a 'saw-tooth' profile (**Figure 2a**). The glide angle remains very steep relative to the slopes of ocean properties (e.g., temperature isotherms) and allows collection of the familiar cross-sections of temperature and salinity (**Figure 3** and **Figure 4**). The glider speed over ground is affected by ocean currents, yielding a variable horizontal resolution that averages about 3 km. Data collection proceeds continuously, in all weather conditions, and the results are transmitted to shore by satellite for immediate evaluation and use. A glider's endurance, autonomy, and maneuverability through the ocean make it an ideal platform for gathering oceanographic data from the interior GOM. These data can be exploited for use in ocean surveillance and prediction systems.

Operational Program

In 2009 HMI began experimenting with using gliders for commercial monitoring of the GOM circulation for the deepwater community. Two glider models with different systems and control architectures were used during the experimental phase. As of 2011, the longest deployment operations have been conducted using a Slocum glider manufactured by Teledyne-Webb Research. Despite the label "autonomous", ocean gliders and, in general, most unmanned marine vehicles seldom operate in a fully automated capacity. A glider is able to monitor and change many aspects of its flight, including attitude and navigational correction. Gliders can gather enormous volumes of data from a wide range of sensors but lack sophisticated abilities to process all the information and act intelligently on the results. The intelligent analysis is supplied by humans who remain a part of the control loop for mission planning and execution.

Operating gliders demands few man-hours relative to equivalent operations conducted using vessels. Most man-hours are committed to vehicle preparation, deployment, and recovery. The glider team consists of technicians who prepare and launch the glider and a pilot who handles flight operations during deployments. A healthy glider requires minimal user intervention and will autonomously execute a programmable mission plan. The basic glider control architecture is outlined in **Figure 2b**. Two-way glider communications are initiated over an Iridium satellite connection to Horizon's flight operations center. During the dive phase, the glider acquires standard CTD data then, after reaching its target depth, returns to the surface, acquires a new GPS fix, and repeats the communication cycle. The data payload is transmitted through the Iridium satellite network. Commands may be queued for automatic upload to the glider or issued by a pilot. The data files are processed to extract scientific data and vital status information on glider location, energy usage, and flight performance (**Figure 2c**). The glider status and recent oceanographic data can be easily visualized and integrated with other observations to assemble a situational awareness of the "ocean space" in which the glider operates. Mission and route planning are then updated based on the latest information. This adaptive approach means that glider missions may change daily to focus on areas with data gaps, repeat a route, or approach new targets of interest. We also take maximum advantage of our existing observational tools, including Lagrangian drifters reporting surface currents, to improve navigational efficiency and target selection.

Glider endurance depends on managing the available energy stored in the lithium-ion batteries. Power demand is greatest for the high-pressure hydraulic pump and the Iridium transceiver, with lesser demands from the pitch motors, GPS transceiver, CTD pump, and altimeter. Power consumption can be minimized by reducing transmitted data payloads and optimizing

flight performance for efficient dive profiles. The altimeter is rarely needed in deepwater operations. Energy usage averages about 5 Amp-hr per day and allows for endurances approaching 120 days. Because forward speed is limited to about 0.5 knots through the water, adverse currents exert a major influence on the glider route. Strong ocean currents are mainly found in the upper 200 m, and simple strategies to overcome adverse currents include limiting dive altitude or steering across the current. We have successfully piloted a glider "upstream" against the prevailing >3.0 knot LC. The tradeoffs are incomplete profile acquisition and additional navigation time. Conversely, favorable currents provide a substantial boost in forward speed over ground.

Observations and Impacts on Operational Monitoring

We describe the oceanographic data collected during a glider survey conducted from April-August 2011, covering a linear distance of 1400 nm (2700 km) and comprising 1000 vertical profiles. Cross-sections of water properties were obtained throughout the upper 1000 m with 2.5 m vertical resolution. The 112-day deployment (14 April to 03 August) spanned a period of intense activity by the Loop Current (LC). The LC invaded northern Mississippi Canyon reaching latitudes north of 28.25 °N, and spawned two eddies - Eddy Galileo on 21 June 2011 and Eddy Hadal on 01 August 2011 (**Figure 5**). During this period, the glider obtained several cross-sections through the LC front and several cyclonic frontal eddies and operated in close proximity to deepwater platforms on the NGOM slope. Major water masses encountered by the glider during this period are identified in the inset of **Figure 6**. Outside the LC and in the upper water column below the mixed layer, the glider encounters water with the characteristics similar to Gulf Common Water (GCW). Inside the Loop Current is found the Subtropical Underwater (SUW; also known as Tropical Water) which is characterized by a pronounced salinity maximum (Rivas, et al., 2005). At intermediate and greater depth (> 200 m), the glider encountered diminishing temperature and salinities. This transitional water mass is sometimes referred to as Tropical Atlantic Central Water (TACW). At depths below 800 m, there is is a salinity minimum (S< 34.8, T=6 °C) which is associated with Antarctic Intermediate Water (AAIW). Water mass properties at 800-1000 m are largely stable and provide a useful standard for calibrating the glider CTD.

Offshore GOM and in the LC

The glider was flown offshore into the deep ocean where it passed through a cyclonic LCFE eddy and into the main body of the Loop Current. LCFEs are regions of vigorous sub-surface upwelling and upward doming of cool water and are often located along the cyclonic side of the Loop Current. They can be identified from their density structure and cyclonic currents. In **Figure 7** we show the results obtained from one such cross-section between 17-29 April. Glider temperature and salinity data clearly reveal the presence of a GOM cold-core cyclone over the lower NGOM slope. The 10 °C isotherm is domed upward by > 100 m over a good portion of the first 100 km cross-section, and the thermocline is compressed into a thinner layer centered at 100 m. One interesting consequence of the density structure within the LCFE can be seen in its effect on sound velocity. The upwelled isotherms and isohalines result in a relative minimum in the sound velocity centered at depths between 500-900 m.

As the glider penetrates into the LC front, the boundary region between the exterior and the tropically-derived LC water mass can be visualized from the location and depth of the 18 °C isotherm (**Figure 7)**. The 18° isotherm plunges from 100 m to 320 m over an along-track distance of 170 km (92 nm). Isopycnals throughout the upper 1000 m are perturbed. The pycnocline subducts along the track and is tilted steeply between 190-200 km along the track and above 150 m. These strong density gradients span a horizontal distance of about 75 km (40 nm). As the glider crosses into the LC, the T-S profiles change distinctly to reflect the presence of the SUW inside the LC front (**Figure 6**). Inside the LC, the surface mixed layer (100 m thick) consists of relatively fresh (35.75 PSS) and relatively warm (> 28 °C) tropical surface water. The surface temperatures of this upper layer vary seasonally. The SUW water mass with maximum salinities (36.8 PSS) is forced beneath the low-density warm tropical surface waters in the LC.

The cross-sections of temperature, salinity, and density may be used to calculate the geostrophic velocity due to differences in geopotential anomaly between adjacent profiles. The result represents the relative change in current profile due to density variations alone, sometimes referred to as the geostrophic shear profile. Problematically, this derived value is only defined perpendicular to a line joining any two profile pairs and is relative to an unknown velocity. A known velocity reference can be calculated, however, from the discrepancy between the glider's dead-reckoned and GPS positions following each dive. The offset represents the depth averaged influence of currents and can be assumed to coincide with the direction of stream flow. With this piece of information, the geostrophic shear can be corrected to form a more complete estimate of the total current. This capability presents a useful opportunity to map the velocity cross-section in the LC front region. The validity of this method depends on several assumptions: flow is conserved along streamlines (no along-stream variation in water properties, and the LC changes slowly over time scales of several days. In addition, the method cannot capture current rotation with depth. We note that in the complex region between LCFE and adjoining LC structure, the flow direction almost certainly rotates with depth.

From cross-sections of velocity we obtain several useful parameters that help characterize the currents within the LC front region. The LC current magnitudes are most intense in the region of strongest horizontal and vertical gradients (**Figure 8**). The maximum current in the upper 50 m exceeds 3.5 knots. Using the 1.5 knot isotach as a reference for the outer edge of the LC, we estimate the distance to the LC core at around 50 km (27 nm). The band of strong currents at this point approaches 120 km (64 nm) in width, but this picture is probably aliased by meandering of the LC over several days. The zone of strongest flow > 3.5 knots is roughly centralized in a narrow band <15 km (8 nm) wide and above 60 m. The maximum current diminishes to < 1.0 knot by 400 m. The appearance of a weak counter flow below 600 m (< 0.5 knots) directly under the LC core is interesting but may be unrealistic, because it is unreasonable to expect flow at depth to align in the same plane as flow at the surface. Focusing attention on the upper few hundred meters, it can be seen from **Figure 9** that the LC current shear is strongest from 150-100 m and coincides with the upper layer of the SUW. The region of the LCFE indicates cyclonic flow approaching > 0.5 knots over the upper 400 m and a band of higher speed > 1.0 knot at a radius of 40 km (21 nm). We place lower confidence on these speeds because the mesoscale eddy progression may exceed the glider speed over ground.

The glider is a useful source of data that augments surface and satellite measurements for use in routine monitoring of general circulation. As an example, we show the overlay of drifter data, sea surface altimetry (SSHA) and the location of the LC frontal boundary as determined by analysis of data on 25 April 2011. The glider trajectory in **Figure 10** corresponds with the cross-sections shown in **Figure 7**. The glider entered the main body of the LC front during 25 April. Substantial mismatch can be seen between the strong gradients in SSHA (which one assumes should be associated with the strongest LC flow) and both the drifter trajectory and the analyzed front location. Far Horizon Drifter #2668 exhibited currents > 1.5 knots along the periphery of a lobe in the western LC front, placed ~20 nm west of the SSHA zero contour. The SSHA zero contour intersects the analyzed front at one point but appears to be in error at most other locations.

A second cross-section through the LC was performed about one month later through the western boundary of the LC on 24-31 May. The glider was directed to enter the LC from its west side, passing through the center of a LCFE and into the LC interior. The LC position had advanced north and west by this time, just prior to developing a lobe that eventually detached as Eddy Galileo on 21 June. The tilt of the isotherms at the beginning of the section indicates the edge of the LCFE along the western (cyclonic) side of the LC. In **Figure 11** we focus attention on the structure of the LC front region. Surface waters of the LC have increased by one degree since April and exceed > 29 °C. Surface salinities are nearly identical to those encountered in April. The presence of interior LC water is indicated by the 18 °C isotherm which dives from 100 – 325 m over the course of 250 km (134 nm). As observed in April, the maximum current in the upper 50 m exceeds 3.5 knots. The front region is narrower relative to the April crossing. The LC core is 25 km (13.5 nm) from the outer edge of the LC (the 1.5 knots isotach). The width of the entire LC itself can be similarly estimated at 80 km (40 nm). Note that the movement of the front during the crossing may broaden the apparent width.

Concurrent trajectories of satellite-tracked drifting buoys (e.g., FHD #2727) passing near the region are generally consistent with current magnitude observed in the LC front at 25 m depths (**Figure 12**). For comparison we show the drift current reported by the glider while it lingers on the surface to complete data transmission. The surface drift results from a combination of processes that influence currents including direct wind-drift, Langmuir circulation, inertial currents, and the LC currents. As a result, the drift and calculated geostrophic current may disagree unless the flow is dominated by strong geostrophic ocean currents. Wind directions between 24-30 May were between 5-15 knot, oriented to the NW, rotating clockwise to the NE on 26-28 May, and then back to W by 31 May. Average correlation is only moderate ($r = 0.65$, 95% confidence).

NGOM slope

The LC pushed northward to > 28 °N by 28 July onto the upper reaches of the NGOM slope and in the vicinity of several platforms in MC. Eddy Hadal shed from the LC on 30 July. The advancing front is shown in **Figure 13** along with glider trajectory and calculated surface geostrophic velocities obtained from the profile data. As the glider gained the upper NGOM slope, maneuvering around platforms in MC, it encountered a weak 0.5 knot shelf current flowing westward along the bathymetric contours between water depths of 500 to 1000 m. During this time, the LC front pushed north and appeared to overrun the glider after 29 July, resulting in intensified currents toward the east. The water properties obtained by the glider indicate that, prior to 29 July, the subsurface water (40-180 m) is generally within the range of GCW, as might be expected outside the LC front. As seen in **Figure 14**, this water is clearly fresher than SUW at the same density range. Based on the surface velocities, the LC appeared to have overrun the glider on 29 July. Strong surface currents (> 3.0 knots) experienced by the glider are only found above 40 m. The water properties, however, reveal a more complex picture. The 29 July profile shows a distinct transition toward fresher water at 40-160 m depth ranges. We speculate that this represents a mixture of GCW and fresher continental shelf waters. Near the surface, water properties are more similar to those found in the LC except for the very thin fresher layer (< 34 PSS) above 8 m. The timing of the transition is concurrent with the progressive

cyclonic rotation of the upper level currents toward the east (> 2.0 knots). One possible explanation for these data is the presence of a cyclonic eddy-like flow advancing with the LC. As this feature overran the glider, the arrival of the trailing side of the CE should result in progressive cyclonic rotation of the currents around to the east and possible circulation of waters that include GCW and/or shelf water entrained from the nearby shelf break. The upper layer of stronger flow appears to be a thinned outer periphery of the LC intruding over the upper slope. The shelf break at this point has been previously identified as a region of vigorous cross-slope exchange (Ohlman, et al., 2001).

Summary and Conclusions

The GOM circulation is dominated by the LC and its associated eddies, which greatly influence circulation over the upper NGOM slope and shelf. Deepwater operators have long recognized the importance of monitoring the LC to maximize safe and efficient operations. The GOM is today among the most highly sampled and monitored deep ocean bodies in the world. Even so, the detailed knowledge about the 3D and 4D structure and intensity of the LC remains unobserved over large portions of the region through which it passes. AUGVs provide a means for sustained measurement of the LC over much of this domain. AUGV technology has a long track record in the research community and is now part of sustained ocean observations in many regions (Todd, et al., 2011). Commercial adoption of this technology is now possible. As we have shown here, AUGVs reveal details of the LC subsurface structure and provide estimates of the width and vertical extent of the strongest current. Such subsurface measurements also capture details about poorly recognized or unexpected meso-scale features that lie in close proximity to the LC and will ultimately result in improved forecasting.

References

Forristall, G.Z., K. J. Schaudt, and C. K. Cooper, 1992, Evolution and kinematics of a loop current eddy in the Gulf of Mexico during 1985, J. Geophys. Res. 97, 2173-2184.

Hamilton, P. , T. J. Berger, J. J. Singer, E. Waddell, J. H. Churchill, R. R. Leben, T. N. Lee, and W. Sturges, 2000: DeSoto Canyon Eddy Intrusion Study, Final Report, Volume II: Technical Report. OCS Study MMS 2000-080, U. S. Department of the Interior, Minerals Management Service, Gulf of Mexico OCS Region, 275 pp.

Leben, R. R, 2005, Altimeter-derived loop current metrics in Circulation in the Gulf of Mexico: Observations and Models, Geophys. Monogr. Ser. Vol. 161, edited by W. Sturges and A. Lugo-Fernandez, pp. 181-201, AGU, Washington, D.C.

Ohlmann, J. C., P. Niiler, C. A. Fox, and R. Leben, 2001, Eddy energy and shelf interactions in the Gulf of Mexico, J. Geophys. Res., 106 (C2), 2605-2620.

Rivas, D. A. Badan and J. Ochoa, 2005, The ventilation of the deep Gulf of Mexico, J. Phys. Oceanogr. 35, 1763-1781.

Sturges, W. and A. Lugo-Fernandez, Eds., 2005, Circulation in the Gulf of Mexico: Observations and Models, Geophysical Monograph Series, Vol.161, 360 pp.

Todd, R. E., D.L. Rudnick, R. Davis, and M. D. Ohman, 2011, Underwater gliders reveal rapid arrival of El Nino effects on California's coast, Geophys. Res. Lett., 38, L03609, doi:10.1029/2010GL046376.

Walker, N. D., "Satellite assessment of Mississippi River plume variability: causes and predictability," Remote Sens. Environ., 1996, vol. 58, no. 1, pp. 21-35.

Wang, D-P., L-Y. Oey, T. Ezer, and P. Hamilton, 2003: Near-surface currents in DeSoto Canyon (1997–99): Comparison of current meters, satellite observation, and model simulation. J. Phys. Oceanogr., 33(1), 313-326.

Vukovich, F. and G. Maul, 1985. Cyclonic eddies in the eastern Gulf of Mexico. J. Phys.Oceanogr. 15:105–117.

Figures

Figure 1. Teledyne-Webb Research Slocum 1000 m autonomous glider.

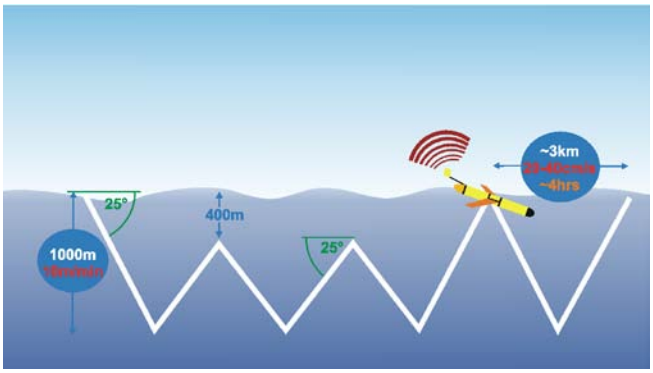

Figure 2a. Schematic dive behavior of a glider. Dive behavior and trajectories are adjustable and typically describe a saw-tooth trajectory with dive angles ~ 25° from horizontal. The linear distance covered in each 4-hour dive is about 3 km at forward speeds of 0.5 knots relative to the water.

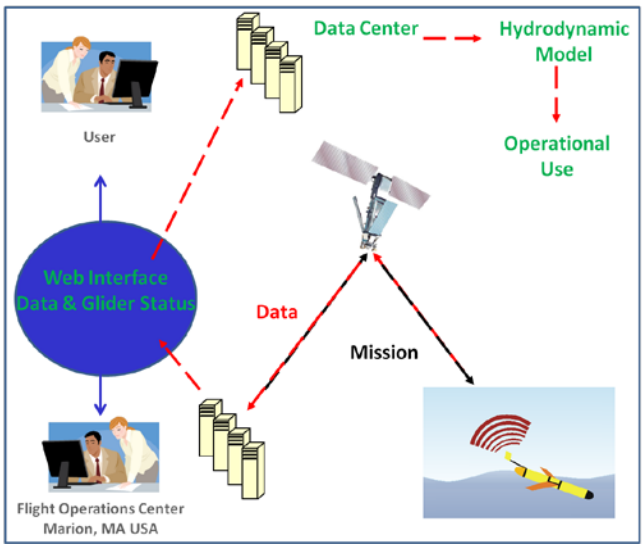

Figure 2b. Simplified command and control architecture. Data (red) and commands (black) are transmitted by Iridium satellite. Status and data are archived and pushed to web-based interfaces. Glider data are incorporated into a forecast model for operational use.

Figure 2c. Glider flight operation status and performance monitor.

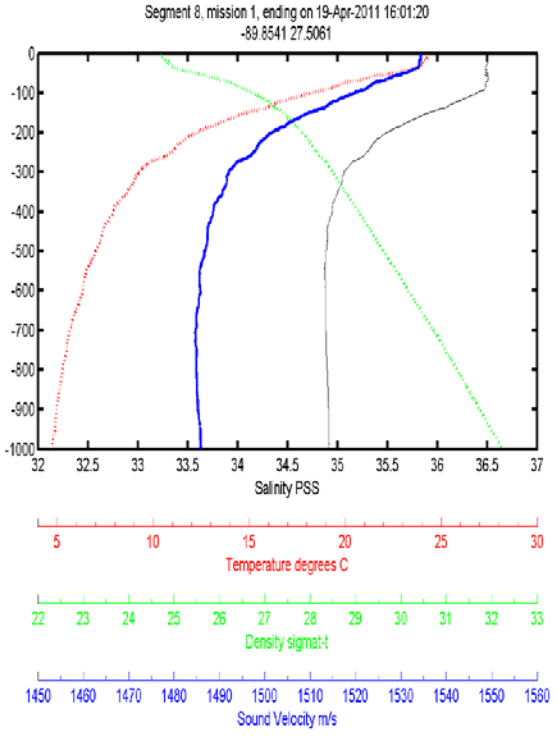

Figure 3. Typical profile of T, S, Sigma-theta, and derived sound velocity.

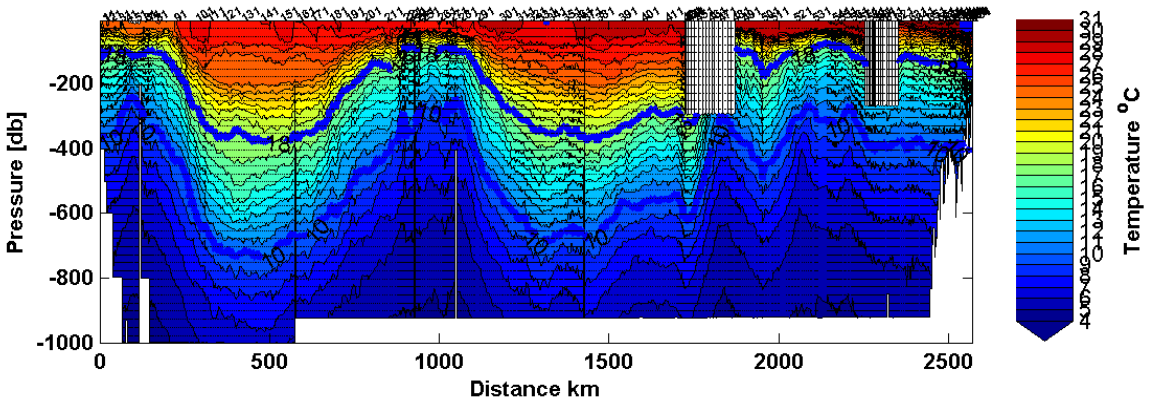

Figure 4. Temperature cross-section in the GOM collected by a glider from April – August 2011. Blank areas indicate truncation of the glider dive profile to a maximum or minimum altitude below the sea surface. Every tenth dive is labeled on the upper x-axis and a dot placed every 25 m in the vertical.

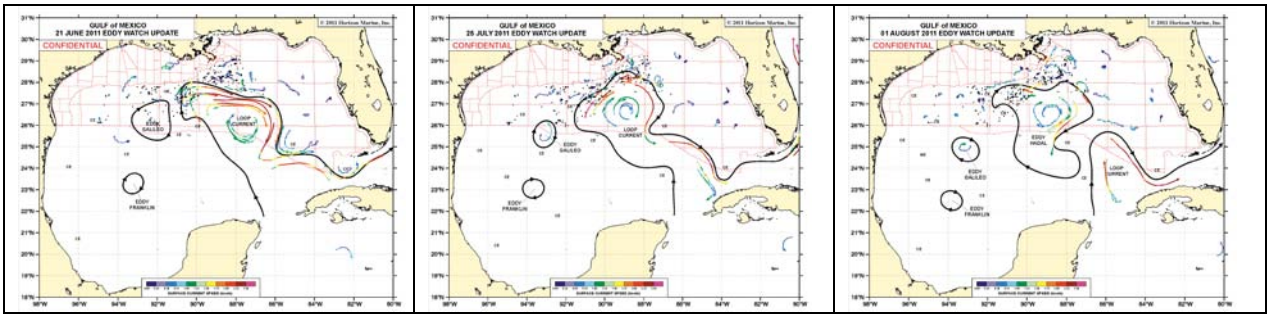

Figure 5. Sequence of LC activity during 2011, including spawning of Eddy Galileo from a peripheral LC lobe on 21 June (left), incursion of the LC to latitudes > 28.5°N on 28 July (center), and shedding of Eddy Hadal by 30 July (right).

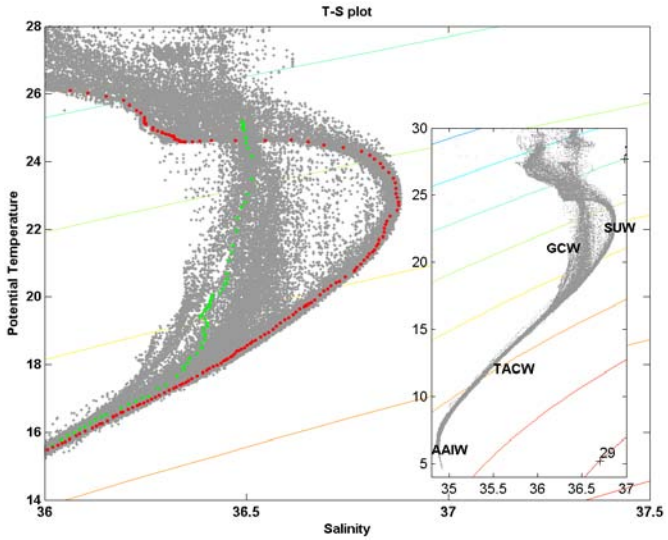

Figure 6. T-S plot of glider data between April-August (gray dots). Major water mass types are identified in the inset figure. The T-S profiles for 25 April (green dots) and 26 April (red dots) are overlaid.

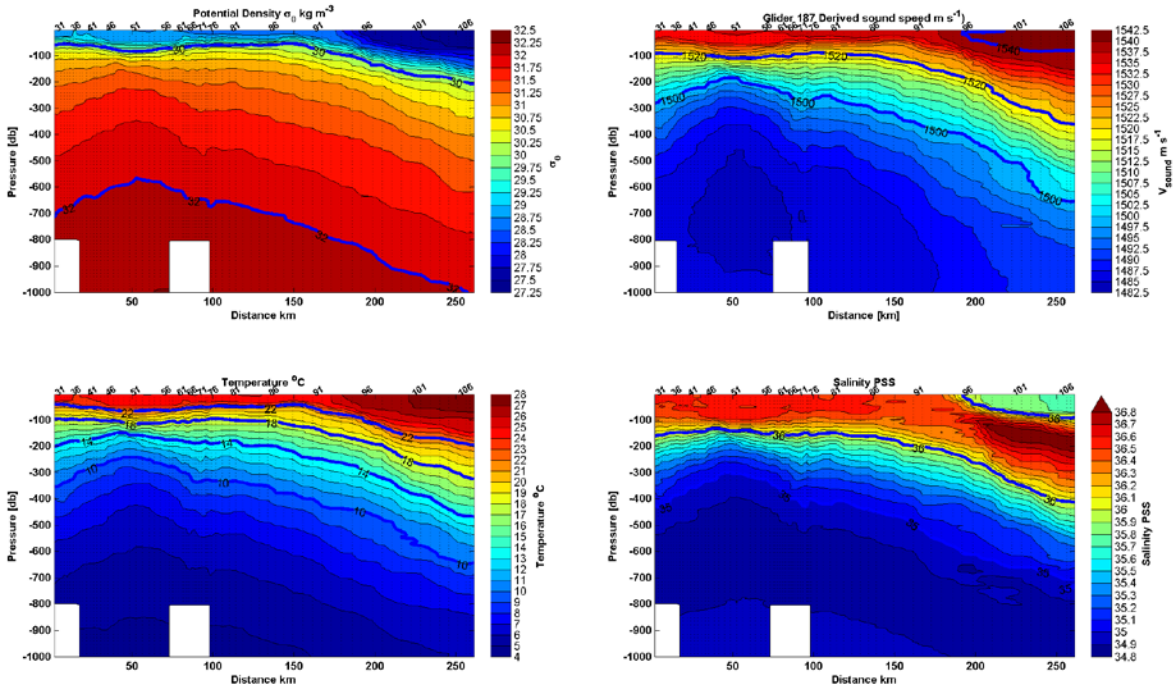

Figure 7. Cross section from 17-29 April from the NGOM slope through the CE and into the LC front region and then LC interior: potential density (top left), sound speed (top right), temperature (bottom left), and salinity (botttom right). Distances are in km along the glider track.

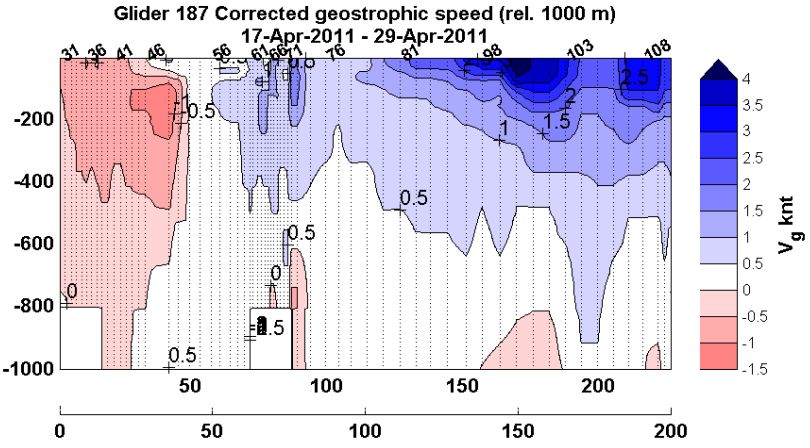

Figure 8. Absolute geostrophic velocity relative to 1000 m. Refer to Figure 10 for the glider path during this crossing. Distances are in km along the glider track (upper x-axis) and cross-stream distance (lower x-axis) which is the projected distance perpendicular to the LC stream flow.

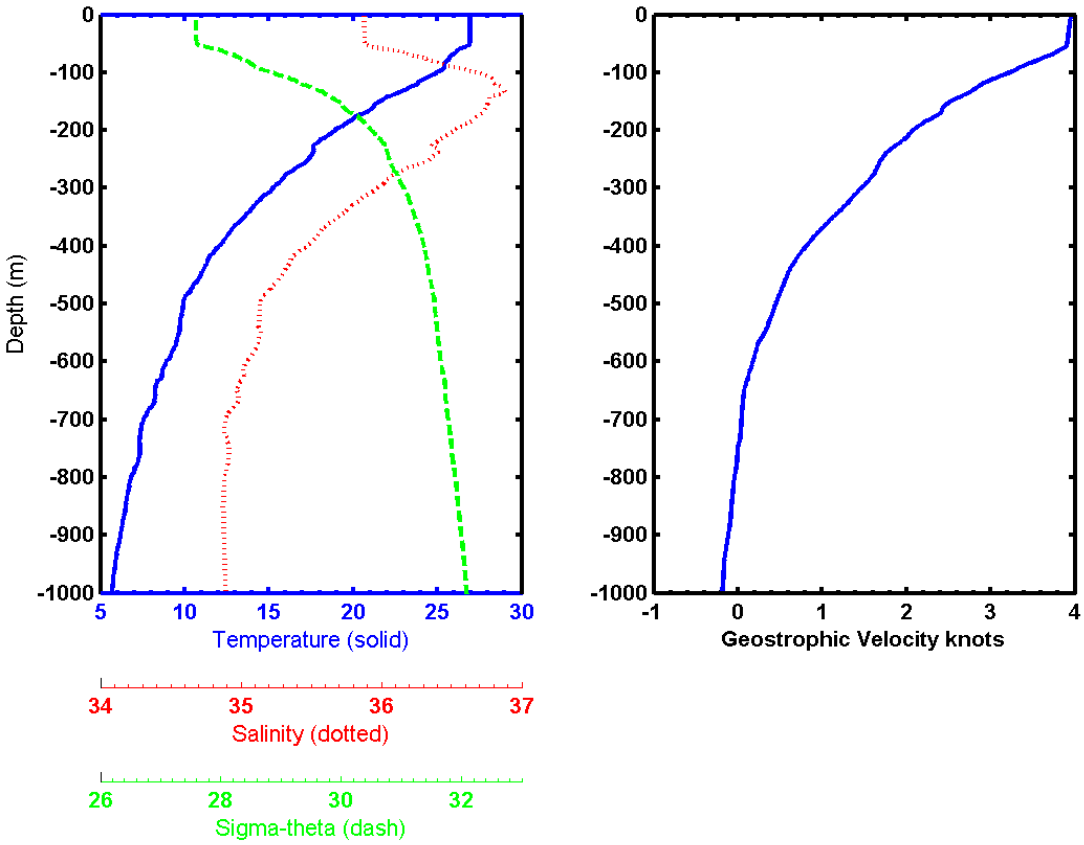

Figure 9. Vertical profiles of T, S, and Sigma-theta collected in the LC core where currents are strongest, and the corresponding geostrophic velocity profile (right).

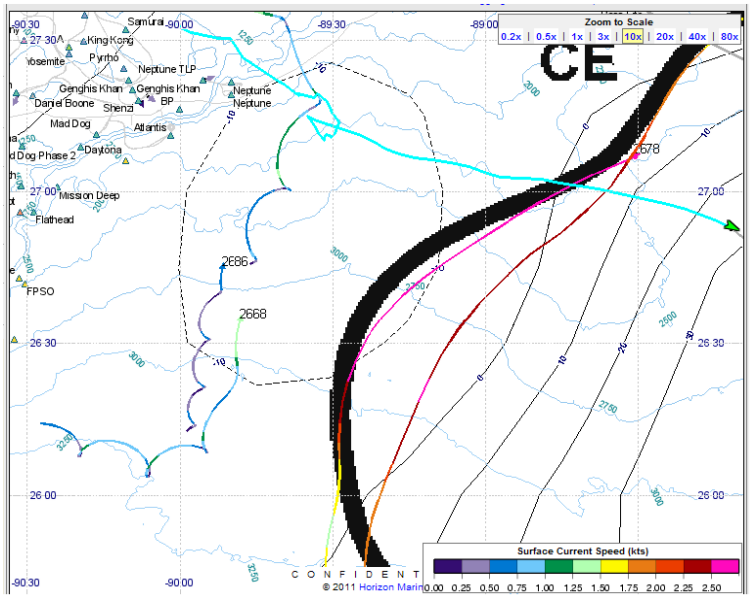

Figure 10. Glider trajectory (aqua blue line) and analysis of Loop Current front position on 25 April 2010. Several drifter trajectories are also shown. The sea surface height altimetry from 25 April is overlaid for comparison.

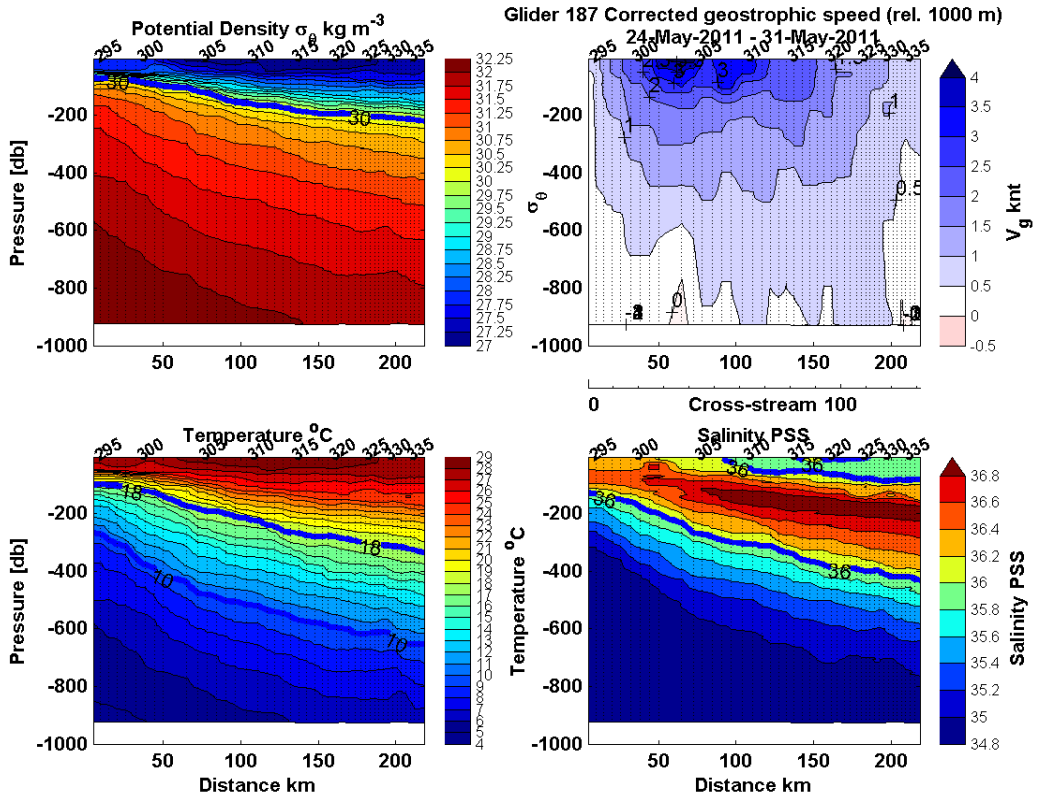

Figure 11. Cross-section from 24-31 May extending from west to east into the LC front region and the LC interior: potential density (top left), absolute geostrophic velocity relative to 1000 m (top right), temperature (bottom left), and salinity (bottom right). Refer to Figure 12 for the glider path during this crossing. Distances are in km along the glider track except for the cross-stream distance (top right) which is the projected distance perpendicular to the LC stream flow.

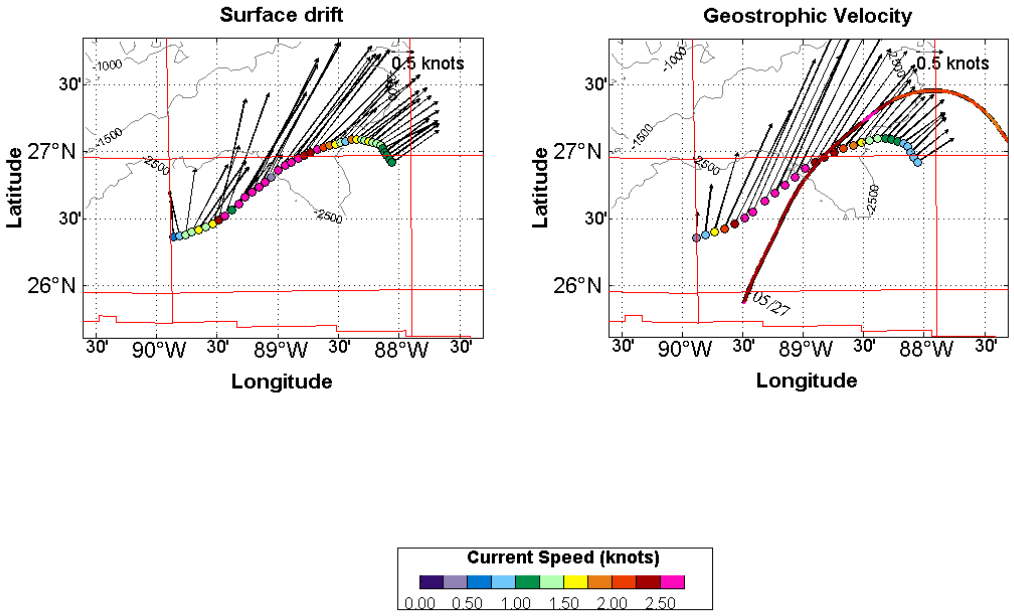

Figure 12. Drift of the glider during the transmission cycle on the surface calculated from successive GPS positions (left), geostrophic velocity at 25 m (right). The trajectory corresponds to the cross-sections presented in Figure 11 from 24 – 31 May. The trajectory and speed of drifter #2727 is overlaid for the period 27-31 May.

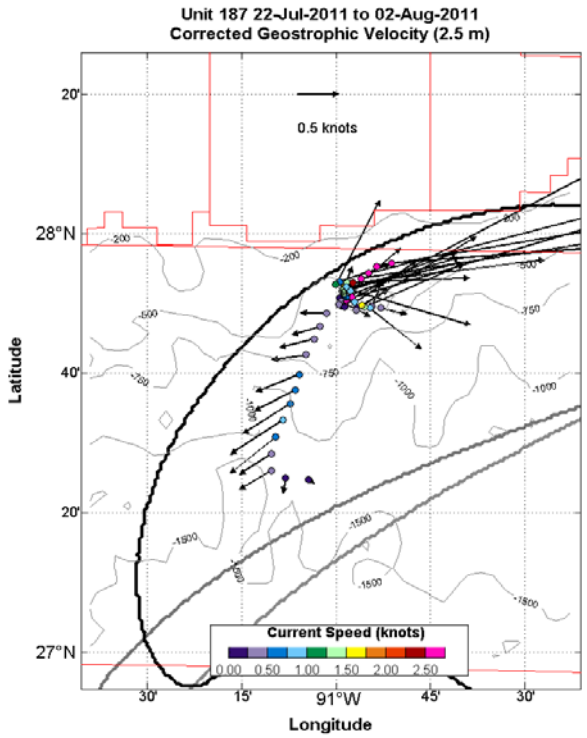

Figure 13. Glider trajectory and geostrophic surface current from 22 July to 02 August. The analyzed LC front positions are overlaid for 26 July (light gray), 27 July (medium gray), and 02 August (dark line). The LC front pushed northward towards its maximum penetration north of 28 °N and onto the outer NGOM shelf (< 200 m isobath) during this period, and the LC front overran the glider location by 29 July.

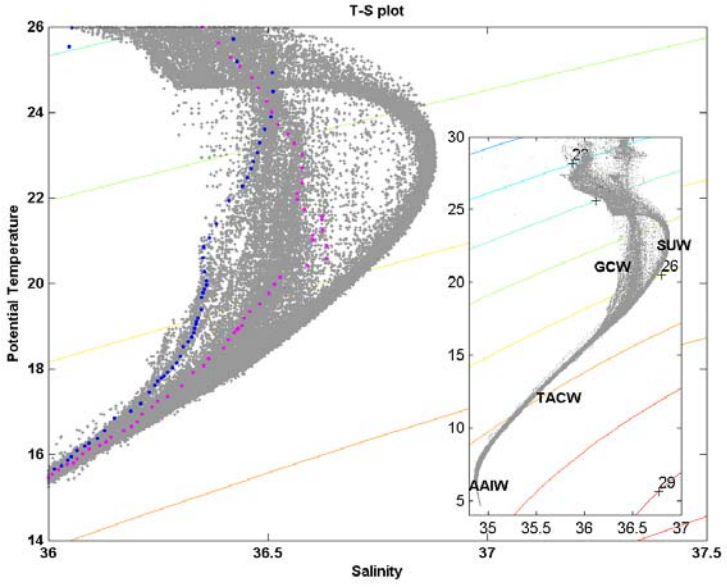

Figure 14. T-S plot of glider data between April-August (gray dots). Major water mass types are identified in the inset figure. The T-S profiles for 22 July (blue dots) and 29 August (magenta dots) are overlaid.